Morphological image sequence processing

Karol Mikula[1], **Tobias Preußer**[2], **and Martin Rumpf**[2]

[1] Department of Mathematics, Slovak University of Technology, Bratislava, Slovakia, e-mail: mikula@vox.svf.stuba.sk
[2] Fakulty 4, Institute for Mathematics, Duisburg University, 47057 Duisburg, Germany, e-mail: preusser@math.uni-duisburg.de, rumpf@math.uni-duisburg.de

Abstract. We present a morphological multi-scale method for image sequence processing, which results in a truly coupled spatio-temporal anisotropic diffusion. The aim of the method is not to smooth the level-sets of single frames but to denoise the whole sequence while retaining geometric features such as spatial edges and highly accelerated motions. This is obtained by an anisotropic spatio-temporal level-set evolution, where the additional artificial time variable serves as the multi-scale parameter. The diffusion tensor of the evolution depends on the morphology of the sequence, given by spatial curvatures of the level-sets and the curvature of trajectories (=acceleration) in sequence-time. We discuss different regularization techniques and describe an operator splitting technique for solving the problem. Finally we compare the new method with existing multi-scale image sequence processing methodologies.

1 Introduction

During the last decade scale-space methods have proven to be useful in image processing, including image denoising, edge enhancement and shape recovery from noisy data [1,25,33, 38]. A given image is thereby considered as initial data to some suitable evolution problem. The artificial time parameter acts as the scale parameter, which guides the user from noisy fine scale representations to enhanced and coarse scale representations of the original image.

Within many applications not only single images but whole image sequences are of particular interest. The observed time period thereby ranges from a few seconds to days, months and years. In medical image processing recent acquisition hardware such as ultrasound (US), magnetic resonance imaging (MRI) and computed tomography imaging (CT) enable for an observation of e.g. the human heart during a cardiac cycle, the flow of a tracer through blood vessels, or the growth of tumors. These image sequences and especially ultrasound data are characterized by high frequent noise typically due to measurement errors of the underlying imaging device. The particular interest in medical applications is understanding of growth and flow phenomena of tissue and the quantitative volume change in time (e.g. blood volume in the heart). Thus one often is interested in the extraction of certain level-surfaces from the data which bound volumes or separate regions of interest. Moreover the extraction of the velocities describing the motion of the level-sets in the sequence, the so called *optical flow*, is desired.

Moreover the method takes into account the velocity in whose direction the level-sets move within the image sequence and finally the acceleration of the level-sets which characterizes this motion in sequence-time. Let us emphasize that the resulting evolution is a truly coupled anisotropic spatio-temporal smoothing process which treats the image sequence as a unit and not as a compilation of single frames.

The paper is organized as follows: First, in Section 2 we discuss some background work on image processing, image sequence processing and the optical flow problem. In Section 3 we review an anisotropic level-set diffusion model for the processing of single frames. This further motivates the modeling of the final evolution. Before we give a detailed description of the new model in Section 5, we will have to discuss the extraction of motion velocities from given image sequences in Section 4. In Section 6 we discuss the robust evaluation of curvatures on level-sets and the discretization by finite elements. Before we draw conclusions in Section 8, we would like to compare the new method with existing image sequence processing methodology in Section 7. In the Appendix we give further details on the spatio-temporal discretization.

2 Related work

Scale Space methods in image processing define an evolution operator $E(t)$ which acts on initial data u_0 and delivers a scale of representations $\{E(t)u_0\}_{t\geq 0}$. The time parameter t serves as the scale parameter that guides from fine scales on the initial data ($t = 0$) to successively coarser and smoother scales. Throughout this paper we will always denote the multi-scale parameter by t whereas – to avoid any confusion – for the sequence-time parameter we will use s, which represents time in the image-sequence data.

The simplest linear image processing model given by the heat equation $\partial_t u - \Delta u = 0$ with the noisy image u_0 as initial

data leads to smooth images but also destroys edges in the image, indicated by high gradients. The proposal of Perona and Malik [24] and the modification of Cattè et al. [7] avoids this drawback considering an evolution problem

$$\partial_t u - \operatorname{div}(G(|\nabla u_\sigma|)\nabla u) = 0,$$

where the diffusion coefficient depends on the magnitude of the gradient of a (regularized) version of the actual image u. Here, $u_\sigma = K_\sigma * u$ is the convolution of the image with a Gaussian kernel K_σ of variance $\sigma > 0$. In contrast to the original Perona/Malik model ($\sigma = 0$) the regularization turns this model into a mathematically well posed problem and moreover it avoids the detection and accentuation of artificial edges which are due to noise. A suitable choice for the diffusion coefficient is $G(s) = (1 + s^2/\lambda^2)^{-1}$ for some $\lambda > 0$. At least formally, decreasing the diffusion coefficient in areas of high gradients then results in a backward diffusion and thus an enhancement of edges, whereas areas of low gradients are smoothed in an isotropic way. The method was improved by Weickert [37] who took anisotropic diffusion into account. Thereby the diffusion is of original Perona/Malik respectively Cattè et al. type in directions of the image gradient (i.e. orthogonal to level-sets) and of linear type in directions tangential to level-sets. This leads to an additional smoothing tangential smoothing of level-sets and enables to amplify intensities or correlations along level-sets. In [26] Preusser and Rumpf applied this type of anisotropic diffusion to visualize arbitrary vector fields. Convergence of a finite element method and finite volume methods were shown by Kačur and Mikula [18] and Mikula and Ramarosy [22]. Furthermore adaptivity was considered in [5,27,19].

In the axiomatic work of Alvarez et al. [1] general nonlinear evolution equations were derived from a set of axioms. Including the axiom of gray value invariance (i.e. the model is supposed to be invariant under monotone transformations of the gray value) lead to a curvature evolution model. Curvature motion has been studied intensively in geometry and physics, where interfaces are driven by surface tension [4,34]. Already in the basic model for mean curvature motion

$$\partial_t u - |\nabla u| \operatorname{div}(\nabla u/|\nabla u|) = 0,$$

singularities in the evolution may occur. In this setting existence of viscosity solutions has been shown independently by Evans and Spruck [13] and Chen et al. [8]. Anisotropic curvature motion has for instance been studied by Belletini and Paolini [6]. Moreover Sapiro proposed a modification of the mean curvature motion model which takes into account the image gradient magnitude [31].

The detection of motion in image sequences, also known as the *optical flow problem*, is one of the fundamental tasks in computer vision and image processing. For two dimensional (2D) images it has been studied extensively in the past [2,3, 30,12,23]. The velocity of a level-set splits up into a component normal to the level-set and a component tangential to it. The extraction of the tangential velocity is in general not well posed [30]. Thus, one has to restrict the set of possible solution velocities and instead work with the *apparent velocity* [15], which arises from locally constant translations in space. As an alternative one might ask for regularizations in terms of elastic stresses or viscous fluid effects [35,20,10, 9,11,14,17], which is computationally expensive and mostly pays off in cases of large deformations in between frames of the sequence, which we rule out in our applications considered here.

The image processing models discussed above do not immediately apply to image sequence processing. Since there is no coupling between successive frames of the sequence in any of the approaches, it is only possible to process the sequence as a collection of steady-images. Still this lacks a correlation of the smoothed versions of the single frames. Therefore modifications of the standard image processing methods have to be taken into account, which introduce a coupling between the frames of the sequence in terms of the velocity or acceleration of the sequence. In the 2D movie multi-scale analysis [15,1] an evolution equation was derived from a set of axioms, which depends on the curvature (given in terms of the eigenvalues and eigenvectors of the shape-operator S, cf. Section 3) of level-sets and the acceleration of the motion:

$$\partial_t u - |\nabla u| F(t, S, \text{accel}).$$

This forms the base for the approaches presented by Sarti et al. in [32] and Mikula et al. in [21]. In Section 7 the latter will be compared to the method being presented in this paper.

3 Review of Anisotropic level-set diffusion in steady-image processing

In this section we will briefly review an anisotropic level-set diffusion model which was originally presented in [28]. As common for level-set models, we deal simultaneously with all level-sets. Although in certain applications our interest is focused on one specific implicit surface, possibly in advance converted from a parametric to an implicit representation.

Let us denote by $u_0 : \Omega \to \mathbb{R}$ the gray value function of the initial image with inscribed level-sets

$$\mathcal{M}_0^c := \{x \in \Omega \,|\, u_0(x) = c\}.$$

We assume u_0 and the set of corresponding implicit surfaces $\{\mathcal{M}_0^c\}_c$ to be noisy and ask for a family of successively smoothed images $\{u(t,\cdot) \,|\, t \in \mathbb{R}_0^+\}$ where $u(t,\cdot) : \Omega \to \mathbb{R}$ and $u(0,\cdot) = u_0(\cdot)$. Throughout this paper Ω will always be the unit square or cube $[0,1]^d$, $d = 2, 3$. The variable t serves as the scale parameter. Thereby, for each gray value c a family of surfaces $\{\mathcal{M}_t^c\}_{t\in\mathbb{R}_0^+}$ is generated, with $\mathcal{M}^c_{(t=0)} = \mathcal{M}_0^c$. Here we assume $u(\cdot,\cdot)$ to be sufficiently smooth and $\nabla u(t,x) \neq 0$ for all $(t,x) \in \mathbb{R}_0^+ \times \Omega$. Indeed, due to the implicit function theorem the corresponding sets $\mathcal{M}_t^c$ then are actually smooth surfaces.

3.1 The Shape Operator

Since our goal is a morphological multi-scale model, we need a characterization of the level-set geometry on images. To this end let us consider the normal to a level-set $N(x) := \frac{\nabla u}{|\nabla u|}$

of some image u. We denote the tangent space by $\mathcal{T}_x\mathcal{M} := (\mathrm{span}\{N(x)\})^\perp$. We compute the Jacobian of the normal

$$DN = (\mathrm{Id} - N \otimes N)\frac{D^2u}{|\nabla u|}$$

on $\mathbb{R}^3$ and consider the restriction

$$S := DN(\mathrm{Id} - N \otimes N)$$

on the tangent space $\mathcal{T}_x\mathcal{M}$. S is a symmetric mapping and on the tangent space $\mathcal{T}_x\mathcal{M}$ it coincides with the *Shape Operator* $S_{\mathcal{T}_x\mathcal{M}}$. Therefore S is characterized by the eigenvalues $\{\kappa^1, \kappa^2, 0\}$ and the eigenvectors $\{v^1, v^2, N\}$. The eigenvalues κ^i correspond to the principal curvatures of the level-set and the eigenvectors v^i are the principal directions of curvature. Thus, the geometry of the level-set is determined by S via its eigenvalues and eigenvectors.

3.2 The anisotropic level-set model

We consider the following type of nonlinear boundary and initial value problem on Ω: Given an initial image $u_0 : \Omega \to \mathbb{R}$ find a family of images $\{u(t,\cdot) : \Omega \to \mathbb{R}\}_{t\in\mathbb{R}^+}$ which obey the following anisotropic evolution equation

$$\begin{aligned} \partial_t u - |\nabla u|\mathrm{div}\left(a^\sigma_{\mathcal{T}_x\mathcal{M}}\frac{\nabla u}{|\nabla u|}\right) = 0 \qquad & \text{in } \mathbb{R}^+\times\Omega, \\ a^\sigma_{\mathcal{T}_x\mathcal{M}}\frac{\partial u}{\partial \nu} = 0 \qquad & \text{on } \mathbb{R}^+\times\partial\Omega, \\ u(0,\cdot) = u_0(\cdot) \qquad & \text{in } \Omega, \end{aligned} \tag{1}$$

where ν denotes the outer normal to Ω. The anisotropic geometric level-set diffusion model should depend on the geometry of the level-sets. Thus it is natural to base the definition of the diffusion coefficient $a^\sigma_{\mathcal{T}_x\mathcal{M}}$ on a regularized version S^σ of the shape operator S. We assume this regularized version diagonalizes with respect to the basis $\{v^{1,\sigma}, v^{2,\sigma}, N^\sigma\}$ having eigenvalues $\{\kappa^{1,\sigma}, \kappa^{2,\sigma}, 0\}$. We then consider the scalar function $G(s) := (1 + s^2/\lambda^2)^{-1}$ from the basic image processing models now acting on S^σ. In matrix representation we thus obtain

$$\begin{aligned} a^\sigma_{\mathcal{T}_x\mathcal{M}} &:= a^\sigma_{\mathcal{T}_x\mathcal{M}}(S^\sigma) \\ &= B_\sigma^T \begin{pmatrix} G(\kappa^{1,\sigma}) & & \\ & G(\kappa^{2,\sigma}) & \\ & & 0 \end{pmatrix} B_\sigma \,, \end{aligned}$$

where $B_\sigma = (v^{1,\sigma}, v^{2,\sigma}, N^\sigma)^T$, i.e. the basis transformation from the regularized frame of principal directions and the normal $\{v^{1,\sigma}, v^{2,\sigma}, N^\sigma\}$ onto the canonical basis $\{e_1, e_2, e_3\}$.

Let us recall that in the function G the parameter λ acts as a steering parameter for the detection of edges. For larger values of λ, more features on a level-set will be regarded as edges. In the standard Perona Malik model the value λ is exactly the switch between forward and backward diffusion.

Remark 1. Although we have based this short review on 3D images and therefore level-sets which are 2D-surfaces, we will present examples of 2D-image-sequences in later sections. The definition of the diffusion tensor of the anisotropic diffusion tensor for 2D images then obviously has the form $B_\sigma^T \mathrm{diag}\{G(\kappa^\sigma), 0\}B_\sigma$, where κ^σ is the regularized curvature of the level-lines.

4 Extracting motion velocities from image sequences

Let us from now on assume, we are concerned with an image sequence. At first, we consider a continuous family of images on some time interval $[0,T]$ each image again defined on $\Omega = [0,1]^d, d = 2,3$, which we will denote by

$$u : Q \to \mathbb{R}, \quad (s,x) \mapsto u(s,x),$$

where Q denotes the sequence-time/space cylinder $Q := [0,T]\times\Omega$. Here and in the following s always denotes the sequence-time parameter and x as before spatial coordinates. Again the perspective of level-sets will play a central role in our model. As before we denote

$$\begin{aligned} \mathcal{M}^c(s) &= \{x \in \Omega \mid u(s,x) = c\}, \\ N(x,s) &= \frac{\nabla u(s,x)}{|\nabla u(s,x)|} \quad \text{if } |\nabla u(s,x)| \neq 0, \end{aligned}$$

the level-set of $u(s,x)$ to level-value $c \in \mathbb{R}$ respectively the normal to this level-set, which now depend on the sequence-time s. Hence we have families of level-sets $\{\mathcal{M}^c(s)\}_{c\in\mathbb{R}}$ which change in sequence-time. Assuming there is some correspondence between consecutive images in the sequence (i.e. the sequence is continuous in sequence-time), it will be an essential part of the new model, to extract the underlying motion, which influences the observed image intensity. Before proceeding to the description of the new time-space coupled smoothing model, we therefore will briefly focus on the extraction of these motion-velocities from the image-sequence. A more detailed discussion can be found in [29].

Suppose

$$v : Q \to \mathbb{R}^d, \quad (s,x) \mapsto v(s,x)$$

is the velocity field generating the motion in space and time. Therefore a single motion trajectory is described by $x(s)$ with

$$\partial_s x(s) = v(s, x(s)).$$

It is obvious that this optical flow problem — the extraction of v from the image data — is an ill posed problem: Any tangential motion, that only moves one level-set within itself cannot be captured by the process. Nevertheless following two assumptions will allow us to derive a formula for the so called *apparent velocity*:

(A1) *Intensities are preserved along motion trajectories:*

$$u(s_0, x(s_0)) = u(s_0+\tau, x(s_0+\tau)) \qquad -s_0 \le \tau \le T - s_0.$$

This assumption is reasonable since it is related to the invariance of the image acquisition device, which usually measures physical quantities. If this physical quantity moves in time, so does the corresponding image intensity.

(A2) *Locally the underlying motion is a translation:*

$$N(s_0, x(s_0)) = N(s_0+\tau, x(s_0+\tau)) \qquad -s_0 \le \tau \le T - s_0.$$

This assumption is of course fulfilled, assuming the scenery consists of solid objects moving in space.

Differentiating these assumptions with respect to τ and evaluating at $\tau = 0$, we get the following two expressions for $v = v_{\rm n}N + v_{\rm tg}$

$$v_{\rm n} = v \cdot N = -\frac{\partial_s u}{|\nabla u|} \qquad \text{if } |\nabla u| \neq 0, \tag{2}$$

$$v_{\rm tg} = -S^{-1}\partial_s N. \tag{3}$$

Equation (2) is an expression for the normal component $v_{\rm n}N = v \cdot NN$ of the velocity. For equation (3) we remember that the Shape Operator S operates on the tangent space $\mathcal{T}_x\mathcal{M}$ and $\partial_s N \in \mathcal{T}_x\mathcal{M}$. Adding the two parts we obtain the *apparent velocity*

$$v_{\rm app} := v_{\rm n} + v_{\rm tg} = -\left(\frac{\partial_s u}{|\nabla u|}N + S^{-1}\partial_s N\right). \tag{4}$$

In 2D this formula was already obtained by Guichard [15,16] although he did not explicitly express it in terms of the intrinsic Shape Operator. From (3) we again see the limitations of the tangential motion capturing, because it involves the inverse of the Shape Operator, which of course may not exist.

Moreover, in many physical applications it will be sufficient to have the normal velocity $v_{\rm n}$, if the observed process gives reason that $v_{\rm tg} = 0$. For example in porous medium flow we already know from the physical model, that the flow will be in direction of the pressure gradient, which in simple settings will be the normal to the level-sets. Also in the situation depicted in Figure 1 we conclude that the normal velocity is sufficient to characterize the motion since the tissue of the human heart will not allow for tangential motions. There we have depicted the extraction of motion velocities from an image sequence showing one ventricle of the human heart during a cardiac cycle. Moreover Figure 2 shows the extraction of the velocity from an artificial data set, in which ellipsoidal level-sets change their half-axes in time.

Given the apparent velocity we can furthermore compute the acceleration of the motion, which is equivalent to the curvature of the apparent trajectory, resulting from the apparent velocity (cf. [15,16])

$$\begin{aligned}\mathrm{accel}(s,x) &:= \partial_\tau v_{\rm app}(s+\tau, x(s+\tau))\Big|_{\tau=0} \\ &= \partial_s v_{\rm app} + (\nabla v_{\rm app})\, v_{\rm app}.\end{aligned} \tag{5}$$

In Figure 1 we have depicted the extraction of motion velocities from an image sequence showing one ventricle of the human heart during a cardiac cycle.

5 Coupled spatio-temporal anisotropic level-set diffusion in image sequence processing

We are now equipped to formulate the new coupled spatio-temporal anisotropic level-set diffusion model. We would like to combine the good edge and corner preserving behavior of the model reviewed in Section 3 with an anisotropic smoothing in sequence-time in direction of the apparent velocity. To this end let us denote the sequence-time/space gradient by $\nabla_{(s,x)} := (\partial_s, \nabla)$ and the corresponding divergence by $\mathrm{div}_{(s,x)} := \partial_s + \nabla$.

Given a noisy image sequence $u_0 : Q \to \mathbb{R}$, we write down the following spatio-temporal level-set problem:

Find $u : \mathbb{R}^+ \times Q \to \mathbb{R}$ *such that in* $\mathbb{R}^+ \times Q$*:*

$$\partial_t u - |\nabla_{(s,x)} u| \mathrm{div}_{(s,x)}\left(A^\sigma \frac{\nabla_{(s,x)} u}{|\nabla_{(s,x)} u|}\right) = 0. \tag{6}$$

We impose the initial condition

$$u(0,\cdot,\cdot) = u_0(\cdot,\cdot) \quad \text{in } Q \to \mathbb{R},$$

and furthermore one of the following boundary conditions

$$\nabla_{(s,x)} u \cdot \nu_{(s,x)} = 0 \quad \text{on } R^+ \times \partial Q, \tag{BC1}$$

$$\left.\begin{aligned} \nabla u(t,s,\cdot)\cdot\nu = 0 \quad & \text{on } \partial\Omega \\ u(\cdot,0,\cdot) = u(\cdot,T,\cdot) \quad & \text{in } \mathbb{R}^+ \text{ and } \Omega, \end{aligned}\right\} \tag{BC2}$$

where $\nu_{(s,x)}$ denotes the outer normal to the sequence-time/space cube Q and ν denotes the outer normal to $\partial\Omega$. The two different boundary conditions have the following meaning. In (BC1) we prescribe generally natural boundary conditions to the whole sequence, i.e. we have no flux across the spatial boundary of the single frames and moreover no flux at the beginning and the end of the sequence. It may be more convenient to impose natural boundary conditions in space and periodicity in sequence-time which is stated in (BC2).

Again the variable t in the problem acts as the scale parameter and we again emphasize that we make a distinction between t and s; s denoting the sequence-time parameter. The definition of the problem indeed increased the dimension of the data by one, which results in 4D respectively 5D problems for 2D respectively 3D image data. In the following sections we will describe how to solve these 4D respectively 5D problems with moderate effort.

It remains to define the diffusion tensor A^σ for the new model. Denoting the tensor product by $v \otimes w := (v_i w_j)_{ij}$, we consider the normalized sequence-time/space velocity vectors $V^\sigma := (1, v^\sigma_{\rm app})/|(1, v^\sigma_{\rm app})|$ based on regularized apparent velocities $v^\sigma_{\rm app}$, and the diffusion coefficient already known from the steady image model to build

$$A^\sigma = a^\sigma_v\, V^\sigma \otimes V^\sigma + \left(\begin{array}{c|c} 0 & 0 \\ \hline 0 & a^\sigma_{\mathcal{T}_x\mathcal{M}}(S^\sigma) \end{array}\right),$$

with $a^\sigma_v = G(|\mathrm{accel}^\sigma|)$. The function $G(s) = (1 + s^2/\lambda^2)$ again is the well known function from image processing (cf. Section 3). With this definition of the diffusion tensor we indeed prescribe a behavior of the evolution that is edge preserving in space but also smoothing the sequence nonlinearly in direction of V^σ. If the acceleration is high the diffusion will be decreased via the function G. This leads to a good preservation of highly curved motion trajectories (i.e. highly accelerated motion) as shown in Figure 3.

In general the decomposition in the definition of A^σ is not orthogonal. Only if the complete apparent velocity $v_{\rm app}$ vanishes, the diffusion tensor reduces to a diagonal matrix. Therefore in general we actually have a coupled diffusion, with a mixed spatio-temporal diffusion component $G(|\mathrm{accel}^\sigma|)V^\sigma \otimes V^\sigma$. This can be observed from the example

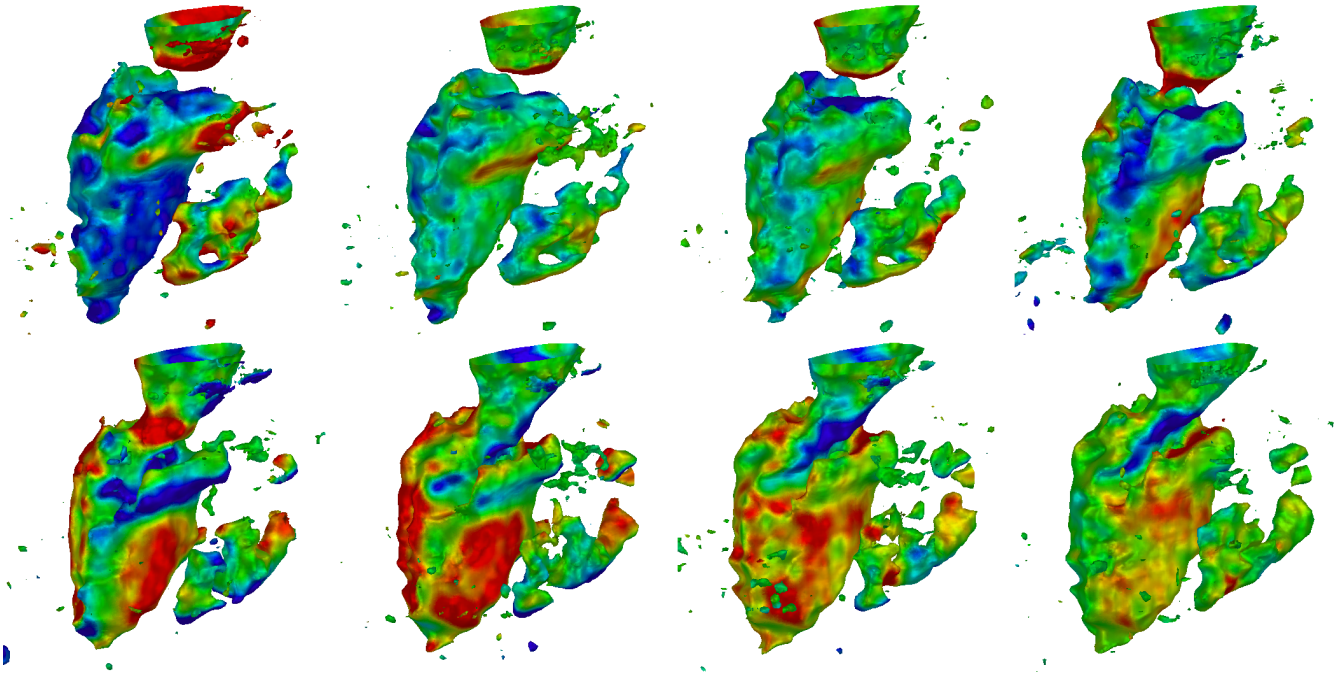

Fig. 1. From an image sequence, taken by an ultrasound device, and showing the left ventricle of the human heart during one cardiac cycle we have extracted the velocities of the underlying motion. From top left to bottom right for successive frames of the sequence one iso-surface of the muscle of the heart is depicted. The coloring codes the normal velocity going inward (red) or outward (blue). Since the tissue of the heart's muscle does not allow for tangential movements it is sufficient to consider the normal velocity in this application.

shown in Figure 4, where we see a diffusion across the sharp edge of the square in direction of the underlying velocity.

Figure 5 shows the evolution of a noisy sample data set under the coupled diffusion model. The image-sequence consists of a continuous function whose level-sets were disturbed randomly in normal direction. The application to real data is shown in Figure 6 where we have extracted one slice of the 3D echocardiographical heart image sequence (cf. Figure 1).

Remark 2. Here and in the sequel we have denoted regularized quantities (like $S^\sigma, v_{\text{app}}^\sigma, \text{accel}^\sigma$) with a superscript σ. We emphasize that we do not distinguish between regularized geometrical quantities and quantities based on regularized data, although they in general do not coincide. In the next section we will focus on the type of regularization we choose in our applications.

6 Discretization and numerical solution

Up to now we have considered image-sequences to be sufficiently smooth in space and time Q. Since in the applications image-sequences arise as a finite sequence of single images (the frames) consisting of arrays of pixels or voxels, we will discretize the model in an appropriate way. For each single frame, we interpret the pixel/voxel values as nodal values on a uniform quadrilateral respectively hexahedral mesh $\mathcal{C}$ covering the whole spatial domain Ω. Moreover since typically the time offset Δs between successive frames is constant in image sequences, we introduce an equidistant lattice in the sequence-time direction. In any coordinate direction, we consider the data to be piece-wise multi-linear, meaning piecewise linear in sequence-time and piece-wise bilinear respectively trilinear in space. To simplify the notation, we will always denote discrete quantities by upper case letters to distinguish them from their continuous correspondence in lower case letters.

6.1 Shape operator and apparent velocity on discrete data

The model presented above makes extensive use of regularized geometric quantities such as the shape operator S^σ and the apparent velocity v_{app}^σ. It is obvious that on noisy image-sequence data a regularization is necessary, but also the definition of these quantities involving higher order derivatives on images which are usually piece-wise constant or rarely given as bilinear respectively trilinear data is not clear. We will therefore in the following focus on these regularized geometric quantities.

For the regularization of the underlying images we have different methods at hand:

- The simplest non-morphological regularization method, which is quite standard in image processing is the convolution of the image with a Gaussian kernel. Thereby one solves a short time step of the heat equation

$$\partial_t \phi - \Delta \phi = 0 \qquad \text{on } Q,$$

  with the given image u as initial value to the problem.
- The morphological analogue of the Gaussian convolution is the mean curvature evolution, which lets all level-sets simultaneously evolve in direction of their normal with a

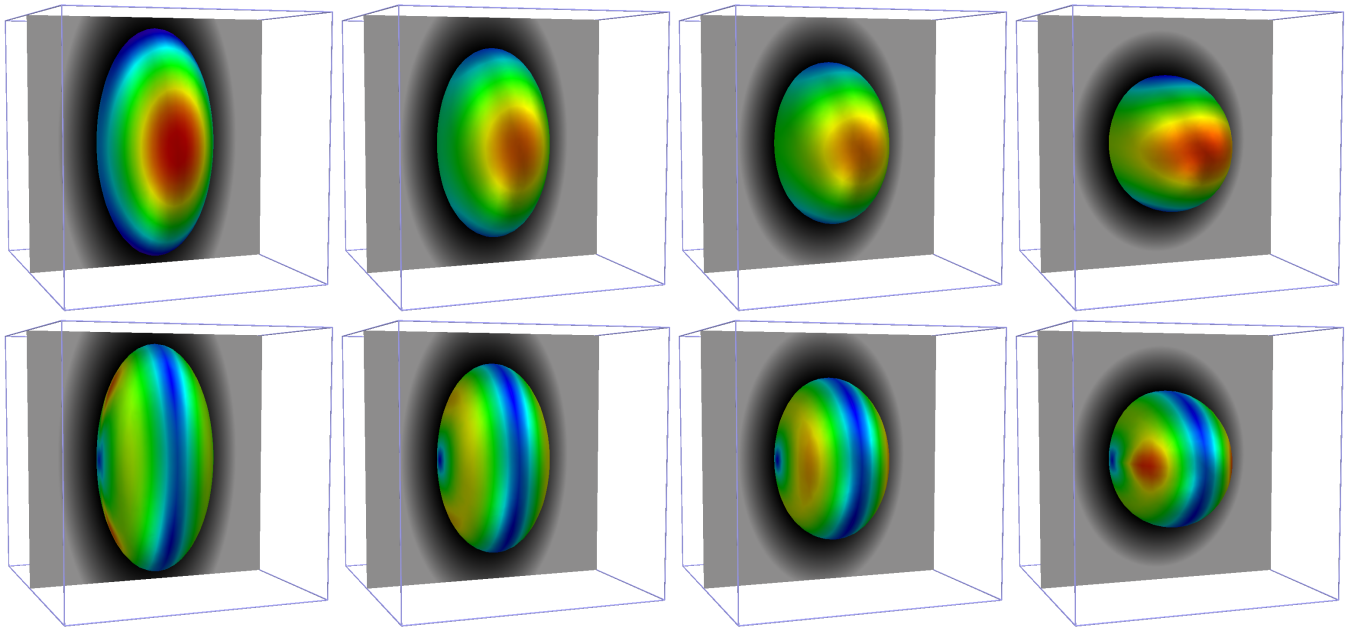

Fig. 2. As a test case we extract the motion from the evolution of ellipsoidal level-sets with oscillating half axes. I.e. we consider the image sequence $\phi(s, x_1, x_2, x_3) := x_1^2/a(s) + x_2^2/b(s) + x_3^2$, where $a(s) := 4s - (1-s)$, $b(s) := s - 4(1-s)$ for $s \in [0,1]$. We have depicted the results of the velocity computation on the same level-set (iso-surface) in different frames of the sequence. In the upper row a color ramp from blue (moving inward) to red (moving outward) indicates the normal component of the velocity. In the lower row the color ramp from blue to red indicates the absolute value of the tangential component of the velocity.

speed according to their mean curvature. The corresponding level-set evolution would be

$$\partial_t \phi - |\nabla\phi| \mathrm{div}\left(\frac{\nabla\phi}{|\nabla\phi|}\right) = 0 \qquad \text{on } Q,$$

again with the given image u as initial value for this parabolic problem.

Both approaches implemented numerically regularize the data, but we are still left with the problem of defining higher order derivatives on piece-wise multi-linear image data. A better approach would be the one used in [28]:

– For each $(s,x) \in \Omega$ take $\mathcal{B}_\sigma(s,x)$ to be some neighborhood of (s,x). Furthermore let $\mathcal{P}$ be some polynomial space of degree greater than one. Now compute the local L^2 projection ϕ of the image data onto $\mathcal{P}$, i.e. solve

$$\int_{\mathcal{B}_\sigma(s,x)} (u(r,y) - \phi(r,y))\, q(r,y)\, dr\, dy = 0 \quad \forall q \in \mathcal{P}.$$

Finally the Shape operator can be computed from the derivatives of the projection.

This last approach is consistent, but also computational very expensive, since a lot of integrations and inversions of small linear systems have to be performed. In the sequel we will therefore describe a third regularization variant (cf. [22]) which is based on convolutions with symmetric smoothing kernels $K_\sigma \in C^\infty$, but additionally uses the convolution property for any derivative D^α

$$\begin{aligned} D^\alpha \left(K_\sigma * u\right)(s,x) &= D^\alpha \int K_\sigma(r,y) u(s-r, x-y)\, dr\, dy \\ &= K_\sigma * D^\alpha u(s,x) = D_x^\alpha K_\sigma * u(s,x). \end{aligned}$$

Since for computations it is essential to have kernels with compact support, we choose

$$K_\sigma(s,x) = \frac{1}{Z} e^{(|x|^2+s^2)/(|x|^2-s^2-\sigma^2)}$$

having support in $\mathcal{B}_\sigma(s,x)$ around (s,x). The constant Z is chosen such that $\int K_\sigma = 1$. We replace the convolution as usual with a weighted summation

$$\begin{aligned} (D^\alpha K_\sigma * u)(s,x) &= \int_{\mathcal{B}_\sigma} D^\alpha K_\sigma(r,y) u(s-r, x-y)\, dr\, dy \\ &= \sum_{E \subset \mathcal{B}_\sigma} u(s_E) \int_E D^\alpha K_\sigma(r,y)\, dy \end{aligned}$$

over the values of u at the center s_E of the involved elements E. The weights are thus obtained by integrating the derivatives of K_σ over the elements $E \subset \mathcal{B}_\sigma(s,x)$ and therefore can be precomputed in advance. Thus we are now equipped with weights for the computation of the derivatives ∂_s, ∇, D^2, on discrete data represented by piece-wise multi-linear functions on the elements of the sequence-time/space grid.

In the above formulas for the computation of v_{app} we have assumed that $\nabla u \neq 0$ and moreover we have made use of the inverse of the shape operator $(S^\sigma)^{-1}$. In general we cannot guarantee that $\nabla u \neq 0$ during the evolution even if the initial data fulfills this assumption (cf. [13]). We therefore have to further regularize the problem by substituting

$$|\cdot| \rightsquigarrow |\cdot|_\epsilon := \sqrt{|\cdot|^2 + \epsilon^2}$$

as proposed by Evans and Spruck in [13]. Moreover in areas where the image is flat at least in one direction (i.e. $\kappa^{i,\sigma} = 0$

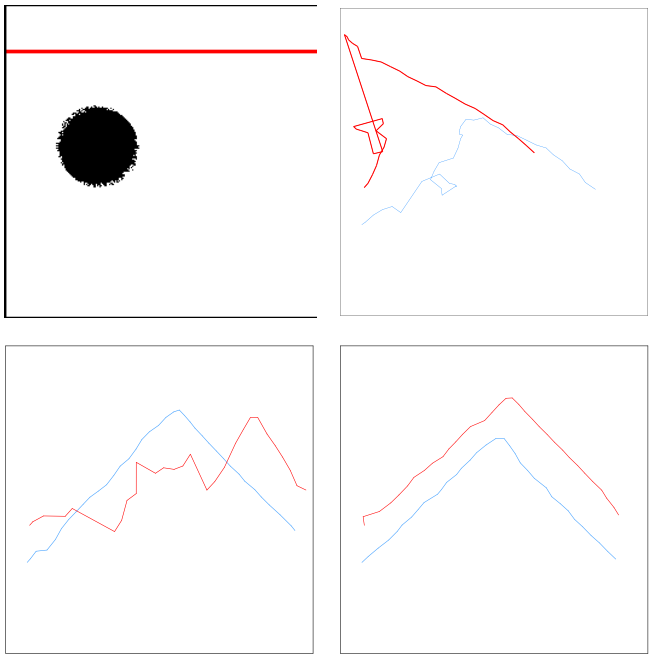

Fig. 3. We show the evolution of single trajectories under the new coupled anisotropic evolution. From a noisy image sequence showing a ball bouncing at some invisible boundary, marked by the red line in the image (top left) we have extracted two motion trajectories (top right). Clearly the velocity is disturbed much and does not at all reflect the underlying motion. In the bottom row we see the same extracted trajectories from the fifth and ninth scale step of the evolution. Clearly the non-accelerated motion has been smoothed much, whereas the rapid velocity change in the middle of the sequence has been preserved very well.

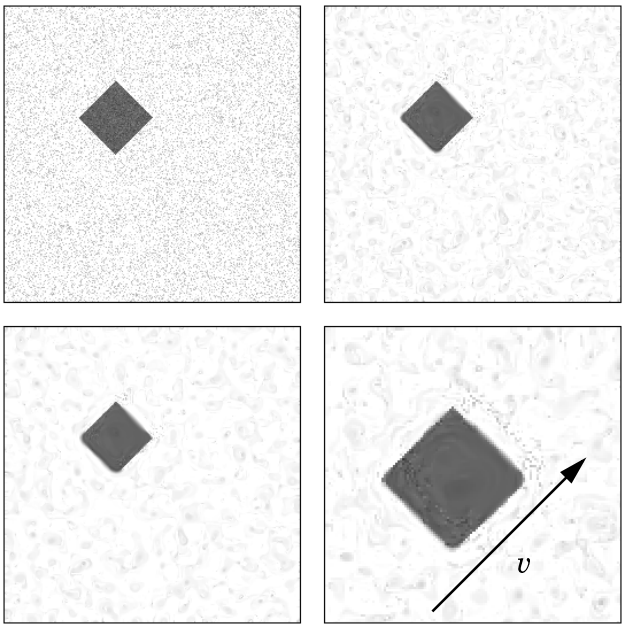

Fig. 4. From a sequence whose frames are piece-wise constant in space, we show the evolution of one single frame. The sequence shows a square bouncing at some invisible object (top left) and we have depicted the third (top right) and the sixth (bottom left) scale step of the evolution. From the magnified section around the square (bottom right) we clearly see, that the coupled diffusion smooths the data across successive slices in direction of the velocity (here diagonally from bottom left to top right). Although the single frames therefore may loose sharpness of edges perpendicular to the velocity, the diffusion makes the whole movie smoother. Obviously, the effect is weaker if the sequence-step-width Δs is smaller since then the pixel/voxel offset between slices is smaller.

for some i), we replace the inverse $(S^\sigma)^{-1}$ by the pseudo-inverse $(S^\sigma)^\dagger$, by inverting S^σ only on $\operatorname{span}\{v^{i,\sigma} | \kappa^{i,\sigma} \neq 0\}$ and extending it trivially again to $\mathcal{T}_x\mathcal{M}$. These are the areas, where we cannot expect the tangent part v_{tg} of the velocity to contain any information, since the image is flat.

Finally, we obtain the following formulas for the Shape operator S^σ, the apparent velocity v^σ_{app} and the acceleration accel^σ:

$$
\begin{aligned}
N^\sigma(s,x) &= \frac{\nabla K_\sigma * u}{|\nabla K_\sigma * u|_\epsilon}(s,x),\\
S^\sigma(s,x) &= \frac{1}{|\nabla K_\sigma * u|_\epsilon}\Big(D^2 K_\sigma * u - \\
&\qquad N^\sigma \otimes (D^2 K_\sigma * u) N^\sigma\Big)(s,x),\\
v^\sigma_{\mathrm{app}}(s,x) &= -\left(\frac{\partial_s K_\sigma * u}{|\nabla K_\sigma * u|_\epsilon} N^\sigma + \right.\\
&\qquad \left. (S^\sigma)^\dagger (\partial_s K_\sigma * N^\sigma)\right)(s,x),\\
\mathrm{accel}^\sigma(s,x) &= \Big((\partial_s K_\sigma * v_{\mathrm{app}}) + \\
&\qquad (\nabla K_\sigma * v_{\mathrm{app}}) v_{\mathrm{app}}\Big)(s,x).
\end{aligned}
$$

6.2 An operator splitting scheme

The coupled problem (6) is a 4D respectively 5D problem for 2D respectively 3D image sequences. Since especially for 3D image sequences we would not like to work with 4D finite elements, we will in the sequel present an operator splitting like scheme which uses appropriate quadrature rules to simplify the solution approach.

We start with the weak formulation of the coupled problem. To this end we discretize in time by a semi-implicit backward Euler scheme, denoting the scale step by Δt and writing $u^n(s,x) = u(n\Delta t, s, x)$. We furthermore test the problem with a function $\psi \in C^\infty(Q)$ and integrate by parts over Q to obtain the time-discrete problem:

Find a family $(u^n)_{n>0}$, $u^n : Q \to \mathbb{R}$ *such that:*

$$
\left(\frac{u^{n+1}-u^n}{\Delta t |\nabla_{(s,x)} u^n|}, \psi\right)_Q - \left(A^{\sigma,n} \frac{\nabla_{(s,x)} u^{n+1}}{|\nabla_{(s,x)} u^n|}, \nabla_{(s,x)} \psi\right)_Q = 0
$$

where $(\cdot,\cdot)_Q$ *denotes the* L^2 *scalar product on* Q *and*

$$
u^0(\cdot,\cdot) = u_0(\cdot,\cdot) \quad \text{in } Q.
$$

The semi-implicity of this scheme results in the evaluation of the nonlinearities at the old time step, i.e. at scale step $n+1$ we take into account $A^{\sigma,n}$ and $|\nabla_{(s,x)} u^n|$.

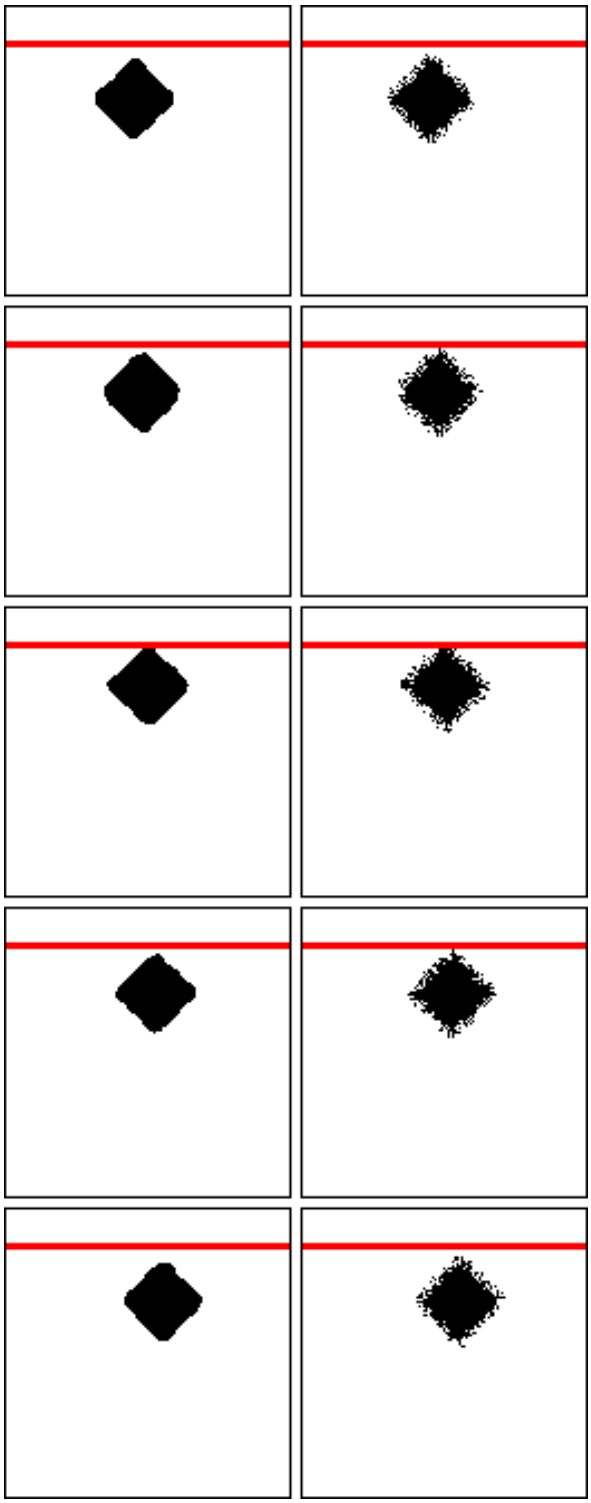

Fig. 5. From a sample data set showing an object bouncing at some solid object, which here is depicted with a red line, we show the coupled multi-scale evolution (cf. Fig. 3). The image data is the continuous function $u_0(s) = |x - d(s)|_1$ to which noise was added, where $d(s)$ is the moving center of the object. The left column shows successive frames of the noisy sequence, whereas the right column shows the same frames after the third scale step of the evolution. We have extracted the sets $\{u(s,x) \leq 0.2\}$ and drawn them in black color. The computations were performed on a 129×129 grid.

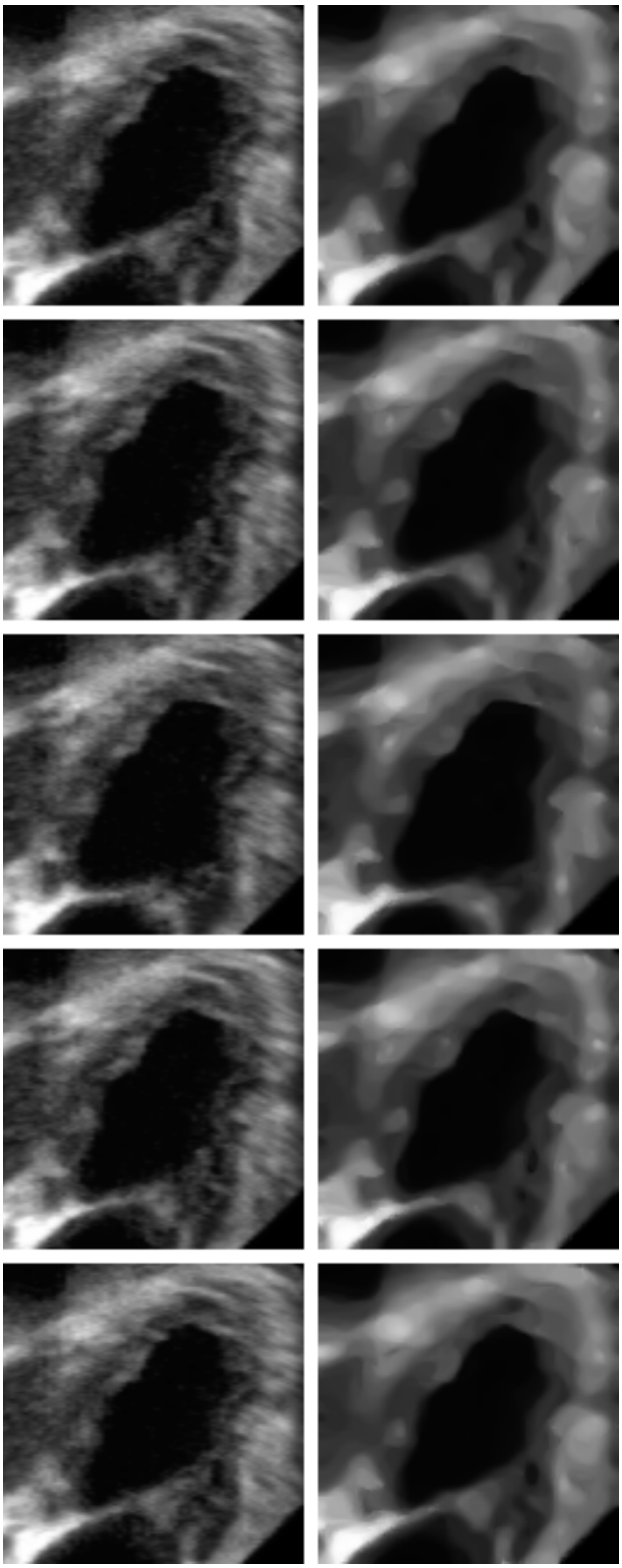

Fig. 6. From the 3D ultrasound image-sequence (cf. Figure 1) we have extracted a 2D image sequence showing a slice through the three-dimensional volume. From top to bottom successive frames of the sequence are depicted. The left column shows the original noisy data, whereas the right column shows the result of the new coupled diffusion model after the third scale step.

$t \in \mathbb{R}_0^+$	Scale
$s \in I$	Sequence time coordinate
$x \in \Omega$	Spatial coordinate
$n \in \mathbb{N}$	Scale step
$i, j = 0, ..., M$	Temporal node index (sequence frame)
$\alpha, \beta = 0, ..., N$	Spatial node index (image voxel)
Δt	Scale-step-width
Δs	Temporal grid width (sequence-step-width)
Δx	Spatial grid width

Table 1. Super- and subscripts in the discretized coupled diffusion problem.

Remark 3. With the definition of $A^{\sigma,n}$ we have for two functions ϕ, ψ

$$\begin{aligned} A^{\sigma,n}&\nabla_{(s,x)}\phi \cdot \nabla_{(s,x)}\psi \\ &= a_v^{\sigma,n}(V^\sigma \cdot \nabla_{(s,x)}\phi)(V^\sigma \cdot \nabla_{(s,x)}\psi) + \\ &\qquad a_{\mathcal{T}_x\mathcal{M}}^{\sigma,n}\nabla\phi \cdot \nabla\psi \\ &= a_v^{\sigma,n}(\partial_s\phi + v_{\text{app}}^\sigma \cdot \nabla\phi)(\partial_s\psi + v_{\text{app}}^\sigma \cdot \nabla\psi) + \\ &\qquad a_{\mathcal{T}_x\mathcal{M}}^{\sigma,n}\nabla\phi \cdot \nabla\psi \\ &=: a_v^{\sigma,n}\frac{D}{\partial s}\phi\frac{D}{\partial s}\psi + a_{\mathcal{T}_x\mathcal{M}}^{\sigma,n}\nabla\phi \cdot \nabla\psi \end{aligned}$$

where $\frac{D}{\partial s} = \partial_s + v_{\text{app}}^\sigma \cdot \nabla = V^\sigma \cdot \nabla_{(s,x)}$ is the material derivative along the apparent motion trajectories.

We proceed with the discretization by formally introducing multi-linear tensor product finite elements on the discrete domain $[0,T] \times \Omega$. To this end let us denote the nodes in sequence time direction s by Latin indices $i, j \in \{0, \dots, M\}$ and the spatial degrees of freedom by Greek multi-indices $\alpha, \beta \in \{0, \dots, N\}^3$. We then have the notation $U^n = (U_0^n, \dots, U_M^n)$ for the nodal values of the nth scale step, where $U_i^n = \{U_{i,\alpha}^n\}_\alpha$ is the discrete image at sequence time i and scale step n. Thus, the identification $u(n\Delta t, i\Delta s, \alpha\Delta x) = U_{i,\alpha}^n$ holds. In Table 6.2 we have collected all the indices which are now in use.

A basis for the multi-linear finite element space is given by

$$\phi_i(s)\ \psi_\alpha(x)$$

where ϕ_i are simple hat functions on the sequence-time lattice and ψ_α also hat functions but on the space-discrete quadtree respectively octtree. We have the following basis decomposition for the nth scale

$$u^n(s,x) = \sum_i \sum_\alpha U_{i,\alpha}^n \phi_i(s)\psi_\alpha(x).$$

From this we derive the standard discrete formulation of the problem, testing with each basis function. Using the last remark, the components of the corresponding matrix system (see Figure 7) in scale step $n+1$ will be given by

$$\left(\frac{\phi_i\psi_\alpha}{|\nabla_{(s,x)}u^n|_\epsilon}, \phi_j\psi_\beta\right)_Q + \tag{MM}$$

$$\Delta t\left(\frac{a_v^{\sigma,n}}{|\nabla_{(s,x)}u^n|_\epsilon}\frac{D}{\partial s}(\phi_i\psi_\alpha), \frac{D}{\partial s}(\phi_j\psi_\beta)\right)_Q + \tag{CP}$$

$$\Delta t\left(\frac{a_{\mathcal{T}_x\mathcal{M}}^{\sigma,n}}{|\nabla_{(s,x)}u^n|_\epsilon}\nabla(\phi_i\psi_\alpha), \nabla(\phi_j\psi_\beta)\right)_Q, \tag{MS}$$

where the integration on Q reduces to the support of the basis functions. The terms correspond to the sequence-time/space mass matrix (MM), a coupled part (CP) consisting of a mixing between sequence-time and space derivatives and the spatial stiffness matrix (MS) multiplied by the sequence-time mass matrix.

The key to simplify these entries is the application of mass lumping in sequence-time [36] and a midpoint quadrature rule in space. The mass lumping results in a diagonalization of the terms (MM) and (MS) in sequence-time.

Furthermore we evaluate the denominator $|\nabla_{(s,x)}u^n|_\epsilon$ at $s = i\Delta s$ always by a central difference $D_{(s,x)}^\pm u_i^n$ in time and therefore can completely split off the sequence-time integration. We obtain

$$\begin{aligned} (\text{MM})_{(\alpha,i),(\beta,j)} &= \int_{(i-1)\Delta s}^{(i+1)\Delta s}\int_\Omega \frac{\phi_i\psi_\alpha\ \ \phi_i\psi_\beta}{|\nabla_{(s,x)}u^n|_\epsilon}\,ds\,dx \\ &\approx \Delta s\left(\frac{\psi_\alpha}{|D_{(s,x)}^\pm u_i^n|_\epsilon}, \psi_\beta\right)_\Omega \end{aligned}$$

Since we have given the nonlinearity $a_{\mathcal{T}_x\mathcal{M}}^{\sigma,n}$ of (MS) on the sequence-time nodes, we can handle this part in a similar way to obtain

$$\begin{aligned} &(\text{MS})_{(\alpha,i),(\beta,j)} \\ &\quad= \Delta t\int_{(i-1)\Delta s}^{(i+1)\Delta s}\int_\Omega a_{\mathcal{T}_x\mathcal{M}}^{\sigma,n}\frac{\phi_i\nabla\psi_\alpha\ \ \phi_i\nabla\psi_\beta}{|\nabla_{(s,x)}u^n|_\epsilon}\,ds\,dx \\ &\quad\approx \Delta t\Delta s\left((a_{\mathcal{T}_x\mathcal{M}}^{\sigma,n})_i\frac{\nabla\psi_\alpha}{|D_{(s,x)}^\pm u_i^n|_\epsilon}, \nabla\psi_\beta\right)_\Omega, \end{aligned}$$

which evaluates $a_{\mathcal{T}_x\mathcal{M}}^{\sigma,n}$ only at the frame i of the sequence.

The remaining term (CP) does not diagonalize in sequence-time. If we split this term up into its parts (according to the last remark), then for each part split off the sequence-time integral by using Fubini's theorem and midpoint integration on the involved sequence-time intervals, we obtain a scheme, that has 3-band block-structure in sequence-time (cf. Appendix 8). The blocks again correspond to the frames in the sequence and moreover the off-diagonal blocks reflect the sequence-time derivatives similar to a difference scheme with stencil $[-1, 2, -1]$ in the sequence-time direction.

The numerical integration of the sequence-time parts considered here separates the sequence-temporal operations from the spatial ones and thus simplifies the resulting matrix.

$$\left(\frac{\phi_i\psi_\alpha}{|\nabla_{(s,x)}u^n|_\epsilon},\phi_j\psi_\beta\right)_Q + \Delta t\left(a_v^{\sigma,n}\frac{\frac{D}{\partial s}(\phi_i\psi_\alpha)}{|\nabla_{(s,x)}u^n|_\epsilon},\frac{D}{\partial s}(\phi_j\psi_\beta)\right)_Q + \Delta t\left(a_{\mathcal{T}_x\mathcal{M}}^{\sigma,n}\frac{\nabla(\phi_i\psi_\alpha)}{|\nabla_{(s,x)}u^n|_\epsilon},\nabla(\phi_j\psi_\beta)\right)_Q$$

↓ Sequence-temporal/spatial mass matrix (MM) ↓ Coupled diffusion terms (CP) ↓ Spatial stiffness matrix (MS)

$$\left(\frac{a_v^{\sigma,n}}{|\nabla_{(s,x)}u^n|_\epsilon}\partial_s(\phi_i\psi_\alpha),\partial_s(\phi_j\psi_\beta)\right)_Q \rightarrow \text{Temporal stiffness matrix } (CP_1)$$

$$\left.\begin{aligned}&+\left(\frac{a_v^{\sigma,n}}{|\nabla_{(s,x)}u^n|_\epsilon}\partial_s(\phi_i\psi_\alpha),v\cdot\nabla(\phi_j\psi_\alpha)\right)_Q\\&+\left(\frac{a_v^{\sigma,n}}{|\nabla_{(s,x)}u^n|_\epsilon}v\cdot\nabla(\phi_i\psi_\alpha),\partial_s(\phi_j\psi_\beta)\right)_Q\end{aligned}\right\}\rightarrow \text{Mixed nonlinear stiffness matrix } (CP_2) \text{ and } (CP_3)$$

$$+\left(\frac{a_v^{\sigma,n}}{|\nabla_{(s,x)}u^n|_\epsilon}v\cdot\nabla(\phi_i\psi_\alpha),v\cdot\nabla(\phi_j\psi_\alpha)\right)_Q \rightarrow \text{Anisotropic spatial stiffness matrix } (CP_4)$$

Fig. 7. The matrix of the system splits up into various parts. The sequence-time/space matrix (upper row, left term) and the spatial stiffness matrix (upper row, right term) lead to diagonal blocks in the resulting scheme, whereas the coupled diffusion terms (upper row, middle term) futher split up (inner box, cf. Appendix 8).

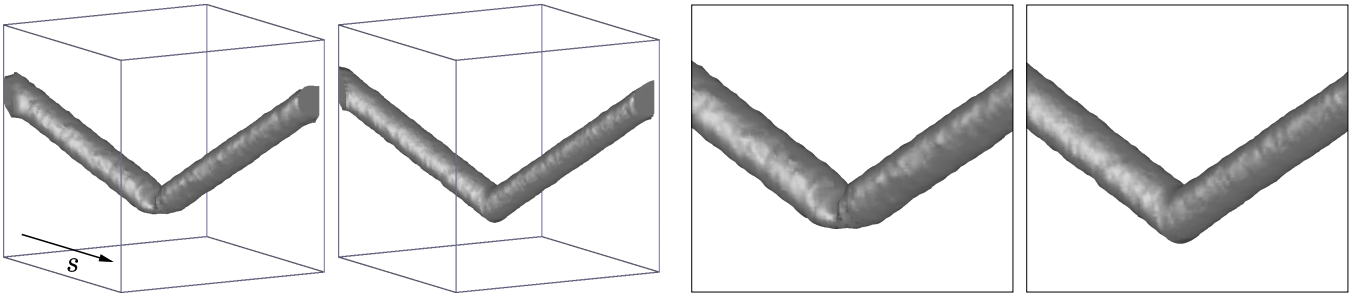

Fig. 8. We compare existing image processing methodology applied to an image-sequence, which shows noisy spherical level-sets bouncing at some solid object (cf. Figure 5). In the left pictures one iso-surface from the 3D representation of the image-sequence smoothed at scale 3 is displayed. The leftmost image shows the result of the model (7) which smooths out the highly accelerated motion of the level-sets. In contrast to that, the anisotropic geometric model (middle left) preserves this behavior quite well. The right images show magnified sections from the iso-surface representations (middle right: model (7), right: anisotropic geometric model).

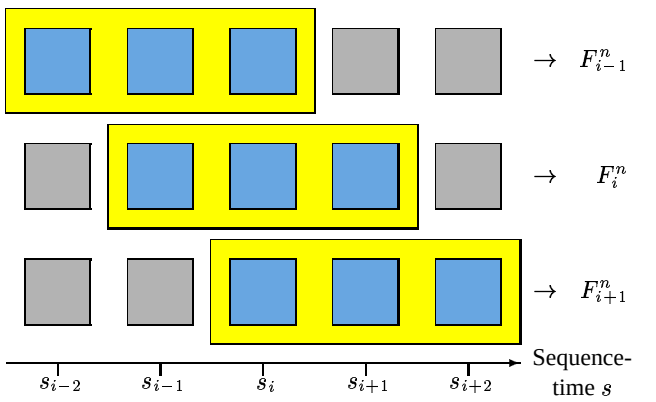

Fig. 9. The block solver considers in each step of the inner frame loop always only three successive images of the sequence. This corresponds to the fact that the resulting system matrix has a 3-band block-structure.

6.3 A Block Solver

The complete matrix of our system now has a 3-band block-structure and therefore we can formally rewrite the discrete problem as (cf. Figure 9):

For each scale $n > 0$ find frames u_i^n such that

$$\langle F_i^n(u_{i-1}^n,u_i^n,u_{i+1}^n),\psi_\alpha\rangle = 0 \qquad \forall\alpha,$$

where the $\langle F_i^n(\cdot,\cdot,\cdot),\psi_\alpha\rangle$ corresponds to the row i of the above derived matrix structure. To solve the system of equations, we use a symmetric block Gauß-Seidel solver which can be sketched as follows:

For each scale $n = 0, 1, \ldots$ do

For each frame $i = 0, 1, \ldots, M$ set $u_i^{n+1,0} = u_i^n$.
For $k = 1, 2, \ldots, k_{\max}$ do

Sweep from left to right: For each frame $i = 0, 1, \ldots, M$ solve for $u_i^{n+1,k}$ the system

$$\langle F_i^n(u_{i-1}^{n+1,k}, u_i^{n+1,k}, u_{i+1}^{n+1,k-1}), \psi_\alpha \rangle = 0.$$

Sweep from right to left: For each frame $i = M, M-1, \ldots, 0$ solve for $u_i^{n+1,k}$ the system

$$\langle F_i^n(u_{i-1}^{n+1,k-1}, u_i^{n+1,k}, u_{i+1}^{n+1,k}), \psi_\alpha \rangle = 0.$$

For each frame $i = 0, 1, \ldots, M$ set $u_i^{n+1} = u_i^{n+1,k_{\max}}$.

If we would set $k_{\max} = 1$ the solution strategy would correspond to an explicit scheme in sequence-time. This is not desirable since the strength of the approach is its nonlinear sequence-time behavior. We therefore fix a small value greater than one for $k_{\max}$ to obtain a better approximation. In our computations we always chose $k_{\max} = 3$. The solution of the subsystems F_i^n is done by a conjugate gradient (CG) method preconditioned by diagonal scaling.

7 Comparison to other methods

In this section we would like to compare some of the image-sequence processing models mentioned in Section 2 with the new model. We will not discuss any steady-image methodology which may be applied to the single frames of the sequence, since a model taking into account velocity and acceleration of an image sequence clearly gives better correlation between successive frames of the sequence.

In [32] Sarti et al. have presented a model for nonlinear image sequence smoothing, which is based on the methodology derived by Guichard in [15]. They took into account the apparent acceleration and the apparent velocity in terms of the *curvature of Lambertian trajectories* (clt) and used the following model:

$$\partial_t u - \mathrm{clt}(u)\mathrm{div}(G(|\nabla u_\sigma|)\nabla u) = 0. \tag{7}$$

The model treats the frames of the sequence separately, but a coupling is given by the modulation of the speed of diffusion via the clt term in front of the divergence. Since the curvature of the trajectories is proportional to the acceleration we conclude that the diffusion will be larger where high acceleration is detected, whereas for non-accelerated motion the equation degenerates to the identity $\partial_t u = 0$.

A similar approach was taken in [21] where the non-morphological Perona-Malik like behavior was replaced by the anisotropic level-set smoothing, which was described in Section 3. Again the frames are treated separately and the coupling is done via the clt term steering the speed of diffusion:

$$\partial_t u - \mathrm{clt}(u)\mathrm{div}\left(a^\sigma_{\mathcal{T}_x\mathcal{M}}(S^\sigma)\frac{\nabla u}{|\nabla u|}\right) = 0.$$

We can characterize the time-smoothing character of both approaches in the following way: The resulting images will be smoother in regions of high acceleration, whereas no smoothing is applied to regions, that move uniformly, non-accelerated. In this sense the behavior of the model presented in this paper is contrary to the clt approaches. First, we have a coupled smoothing, where the sequence is treated as a whole, second, the sequence-time diffusion is decreased if the trajectory has high curvature. On one hand, this results in a smoothing of the images even if the motion is non-accelerated. The important features are then spatial corners and edges. On the other hand accelerated motions especially with nearly discontinuous velocities will be preserved much better.

8 Conclusions

We have presented a new morphological anisotropic smoothing approach for image sequences, which takes into account temporal and spatial curvature information. The multi-scale diffusion thereby is truly coupled in sequence-time and space and the anisotropy directions correspond to the apparent direction of motion in sequence-time and to principal directions of curvature in space. The diffusivity is decreased in areas of high curvature which results in a good preservation of spatial corners and edges as well as highly accelerated motions in sequence-time.

The discretization takes into account a mass lumping in sequence-time and a suitable mid-point integration rule in the corresponding sequence-time intervals. Therefore the matrix scheme resulting from a tensor product multi-linear finite element approach in sequence-time and space has a 3-block structure, where the single blocks correspond to the frames in the sequence. This makes a treatment with moderate effort feasible even for 3D image sequences, which would result in a 5D problem.

On the web site

`http://www.numerik.math.uni-duisburg.de/exports/anisoseq/`

more examples and movies showing image sequences denoised by the new model are available.

Acknowledgments

We thank G. Dziuk and J. Weickert for inspiring discussions on the topic. We furthermore acknowledge C. Lamberti from DEIS, Bologna University and TomTec Imaging Systems for providing the ultrasound image data shown in Figure 1.

Appendix. Operator splitting in the coupled sequence-time/space problem

Within our explanations in Section 6.2 we have claimed that the resulting matrix scheme has a 3-band block structure. So far this has only been shown for a part of the resulting matrix.

Let us recall that the matrix entries of the resulting system are given by

$$\left(\frac{\phi_i\psi_\alpha}{|\nabla_{(s,x)}u^n|_\epsilon},\phi_j\psi_\beta\right)_Q + \quad \text{(MM)}$$

$$\Delta t\left(\frac{a_v^{\sigma,n}}{|\nabla_{(s,x)}u^n|_\epsilon}\frac{D}{\partial s}(\phi_i\psi_\alpha),\frac{D}{\partial s}(\phi_j\psi_\beta)\right)_Q + \quad \text{(CP)}$$

$$\Delta t\left(\frac{a_{T_x\mathcal{M}}^{\sigma,n}}{|\nabla_{(s,x)}u^n|_\epsilon}\nabla(\phi_i\psi_\alpha),\nabla(\phi_j\psi_\beta)\right)_Q. \quad \text{(MS)}$$

In Section 6.2 it has become clear that together with mass lumping in sequence time, the terms (MM) and (MS) only lead to diagonal block-entries in the resulting system. In the following we will show that (CP) leads to two off-diagonal blocks, such that the final matrix has a 3-band block structure. According to the remark on page 9 we split up the term (CP) to

$$\begin{aligned}(\mathrm{CP})_{(i,\alpha),(j,\beta)} \quad & (8)\\ = \Delta t\left(\frac{a_v^{\sigma,n}}{|\nabla_{(s,x)}u^n|_\epsilon}\partial_s(\phi_i\psi_\alpha),\partial_s(\phi_j\psi_\beta)\right)_Q & \quad (\mathrm{CP}_1)\\ + \Delta t\left(\frac{a_v^{\sigma,n}}{|\nabla_{(s,x)}u^n|_\epsilon}\partial_s(\phi_i\psi_\alpha),v\cdot\nabla(\phi_j\psi_\alpha)\right)_Q & \quad (\mathrm{CP}_2)\\ + \Delta t\left(\frac{a_v^{\sigma,n}}{|\nabla_{(s,x)}u^n|_\epsilon}v\cdot\nabla(\phi_i\psi_\alpha),\partial_s(\phi_j\psi_\beta)\right)_Q & \quad (\mathrm{CP}_3)\\ + \Delta t\left(\frac{a_v^{\sigma,n}}{|\nabla_{(s,x)}u^n|_\epsilon}v\cdot\nabla(\phi_i\psi_\alpha),v\cdot\nabla(\phi_j\psi_\alpha)\right)_Q. & \quad (\mathrm{CP}_4)\end{aligned}$$

Again we inspect these terms separately. The first component (CP_1) is the elliptic sequence-time term. Let us perform the integration:

$$\begin{aligned}&(\mathrm{CP}_1)_{(i,\alpha),(j,\beta)}\\ &= \Delta t\int_0^T\int_\Omega \frac{a_v^{\sigma,n}}{|\nabla_{(s,x)}u^n|_\epsilon}\partial_s(\phi_i\psi_\alpha)\partial_s(\phi_j\psi_\beta)\,dx\,ds\\ &\approx \Delta t\sum_k \int_{k\Delta s}^{(k+1)\Delta s}\partial_s\phi_i\,\partial_s\phi_j\,ds\int_\Omega\frac{(a_v^{\sigma,n})_k}{|D^+_{(s,x)}u_k^n|_\epsilon}\psi_\alpha\,\psi_\beta\,dx,\end{aligned}$$

where we assume $a_v^{\sigma,n}$ to be constant over each sequence-time interval $[k\Delta s,(k+1)\Delta s]$ and denoted by $(a_v^{\sigma,n})_k$, and $D^+_{(s,x)}u_k^n$ is the spatio-temporal-gradient evaluated on such an interval. Since the support of $\partial_s\phi_i$ and $\partial_s\phi_j$ only overlap in the case $|i-j|\le 1$ we conclude that the resulting matrix may only have 3-band structure, where the entries in row i are approximated by

$$\begin{aligned}\Bigg[&-\frac{\Delta t}{\Delta s}\left(\int_\Omega\frac{(a_v^{\sigma,n})_{i-1}\psi_\alpha\,\psi_\beta}{|D^+_{(s,x)}u^n_{i-1}|_\epsilon}\right)_{\alpha,\beta},\\ &\frac{\Delta t}{\Delta s}\left(\int_\Omega\frac{[(a_v^{\sigma,n})_{i-1}+(a_v^{\sigma,n})_i]\psi_\alpha\,\psi_\beta}{|D^\pm_{(s,x)}u^n_i|_\epsilon}\right)_{\alpha,\beta},\\ &-\frac{\Delta t}{\Delta s}\left(\int_\Omega\frac{(a_v^{\sigma,n})_i\psi_\alpha\,\psi_\beta}{|D^+_{(s,x)}u^n_i|_\epsilon}\right)_{\alpha,\beta}\Bigg],\end{aligned}$$

where we again have used the central derivative $D^\pm_{(s,x)}u_i^n$ in the diagonal element.

The second and third term (CP_2) and (CP_3) consist of mixed derivatives in sequence-time and space. If the temporal diffusion coefficient $a_v^{\sigma,n}$ was constant, these terms would vanish for symmetry reasons. But since we have built the new model upon nonlinear temporal diffusion, we have to take into account these terms. Again due to symmetry reasons, we only have to take into account the temporal diagonal

$$\begin{aligned}&((\mathrm{CP}_2)+(\mathrm{CP}_3))_{(i,\alpha),(j,\beta)}\\ &= \Delta t\int_0^T\int_\Omega\frac{a_v^{\sigma,n}\partial_s(\phi_i\psi_\alpha)}{|\nabla_{(s,x)}u^n|_\epsilon}v\cdot\nabla(\phi_i\psi_\beta)\\ &\qquad+\frac{a_v^{\sigma,n}\partial_s(\phi_i\psi_\beta)}{|\nabla_{(s,x)}u^n|_\epsilon}v\cdot\nabla(\phi_i\psi_\alpha)\,dx\,ds\\ &\approx \Delta t\Delta s\int_\Omega\frac{[(a_v^{\sigma,n})_{i-1}-(a_v^{\sigma,n})_i]}{|D^\pm_{(s,x)}u_i^n|}\\ &\qquad(\psi_\alpha\,v\cdot\nabla\psi_\beta+v\cdot\psi_\alpha\,\psi_\beta)\,dx\end{aligned}$$

Finally we have the spatial anisotropic elliptic term (CP_4) which can be handled in exactly the same way as before (MM) and (MS) to obtain

$$\begin{aligned}&(\mathrm{CP}_4)_{(i,\alpha),(j,\beta)}\\ &= \Delta t\Delta s\int_\Omega\frac{[(a_v^{\sigma,n})_{i-1}+(a_v^{\sigma,n})_i]}{|D^\pm_{(s,x)}u_i^n|}v\cdot\nabla\psi_\alpha\,v\cdot\nabla\psi_\beta\,dx.\end{aligned}$$

Adding up all the terms (MM) + $\sum_{i=1}^4(\mathrm{CP}_i)$ + (MS), we obtain the stiffness matrix which is then treated by the block solver as shown in Section 6.3.

References

1. L. Alvarez, F. Guichard, P. L. Lions, and J. M. Morel. Axioms and fundamental equations of image processing. *Arch. Ration. Mech. Anal.*, 123(3):199–257, 1993.
2. L. Alvarez, J. Weickert, and J. Sánchez. A scale–space approach to nonlocal optival flow calculations. In M. Nielsen, P. Johansen, O. F. Olsen, and J. Weickert, editors, *Scale-Space Theories in Computer Vision. Second International Conference, Scale-Space 1999, Corfu, Greece, September 1999*, Lecture Notes in Computer Science; 1682, pages 235–246. Springer, 1999.

3. L. Alvarez, J. Weickert, and J. Sánchez. Reliable estimation of dense optimal flow fields with large displacements. *Int. J. of Computer Vision*, folgt:folgt, folgt.
4. S. B. Angenent and M. E. Gurtin. Multiphase thermomechanics with interfacial structure 2, evolution of an is othermal interface. *Arch. Rational Mech. Anal.*, 108:323–391, 1989.
5. E. Bänsch and K. Mikula. A coarsening finite element strategy in image selective smoothing. *Computing and Visualization in Science*, 1:53–63, 1997.
6. G. Bellettini and M. Paolini. Anisotropic motion by mean curvature in the context of finsler geometry. *Hokkaido Math. J.*, 25:537–566, 1996.
7. F. Catté, P.-L. Lions, J.-M. Morel, and T. Coll. Image selective smoothing and edge detection by nonlinear diffusion. *SIAM J. Numer. Anal.*, 29(1):182–193, 1992.
8. Y.-G. Chen, Y. Giga, and S. Goto. Uniqueness and existence of viscosity solutions of generalized mean curvature flow equations. *J. Diff. Geom.*, 33(3):749–786, 1991.
9. G. E. Christensen, S. C. Joshi, and M. I. Miller. Volumetric transformations of brain anatomy. *IEEE Trans. Medical Imaging*, 16(6):864–877, 1997.
10. G. E. Christensen, R. D. Rabbitt, and M. I. Miller. Deformable templates using large deformation kinematics. *IEEE Trans. Medical Imaging*, 5(10):1435–1447, 1996.
11. C. A. Davatzikos, R. N. Bryan, and J. L. Prince. Image registration based on boundary mapping. *IEEE Trans. Medical Imaging*, 15(1):112–115, 1996.
12. R. Deriche, P. Kornprobst, and G. Aubert. Optical–flow estimation while preserving its discontinuities: A variational approach. In *Proc. Second Asian Conf. Computer Vision (ACCV '95, Singapore, December 5–8, 1995)*, volume 2, pages 290–295, 1995.
13. L. Evans and J. Spruck. Motion of level sets by mean curvature I. *J. Diff. Geom.*, 33(3):635–681, 1991.
14. U. Grenander and M. I. Miller. Computational anatomy: An emerging discipline. *Quarterly Appl. Math. LVI*, pages 617–694, 1998.
15. F. Guichard. *Axiomatisation des analyses multi-échelles d́images et de films*. PhD thesis, University Paris IX Dauphine, 1994.
16. F. Guichard. A morphological, affine, and galilean invariant scale–space for movies. *IEEE Transactions on Image Processing*, 7(3):444–456, 1998.
17. S. C. Joshi and M. I. Miller. Landmark matching via large deformation diffeomorphisms. *IEEE Trans. Medical Imaging*, 9(8):1357–1370, 2000.
18. J. Kačur and K. Mikula. Solution of nonlinear diffusion appearing in image smoothing and edge detection. *Appl. Numer. Math.*, 17 (1):47–59, 1995.
19. Z. Kriva and K. Mikula. An adaptive finite volume scheme for solving nonlinear diffusion equations in image processing. *J. Vis. Comm. and Image Repres.*, 13:22–35, 2002.
20. F. Maes, A. Collignon, D. Vandermeulen, G. Marchal, and P. Suetens. Multi–modal volume registration by maximization of mutual information. *IEEE Trans. Medical Imaging*, 16(7):187–198, 1997.
21. K. Mikula, T. Preußer, M. Rumpf, and F. Sgallari. On anisotropic geometric diffusion in 3D image processing and image sequence analysis. In *Trends in Nonlinear Analysis*, pages 305–319. Springer, 2002.
22. K. Mikula and N. Ramarosy. Semi–implicit finite volume scheme for solving nonlinear diffusion equations in image processing. *Numerische Mathematik*, 2001.
23. H. H. Nagel and W. Enkelmann. An investigation of smoothness constraints for the estimation of displacement vector fields from images sequences. *IEEE Trans. Pattern Anal. Mach. Intell.*, 8:565–593, 1986.
24. P. Perona and J. Malik. Scale space and edge detection using anisotropic diffusion. In *IEEE Computer Society Workshop on Computer Vision*, 1987.
25. P. Perona and J. Malik. Scale space and edge detection using anisotropic diffusion. *IEEE Trans. Pattern Anal. Mach. Intell.*, 12:629–639, 1990.
26. T. Preußer and M. Rumpf. Anisotropic nonlinear diffusion in flow visualization. In *Proceedings Visualization 1999*, pages 325–332, 1999.
27. T. Preußer and M. Rumpf. An adaptive finite element method for large scale image processing. *J. Vis. Comm. and Image Repres.*, 11:183–195, 2000.
28. T. Preußer and M. Rumpf. A level set method for anisotropic diffusion in 3D image processing. *SIAM J. Appl. Math.*, 62(5):1772–1793, 2001.
29. T. Preußer and M. Rumpf. Extracting motion velocities from 3D image sequences and coupled spatio-temporal smoothing. In *Proceedings Visual Data Analysis*, 2003, to appear.
30. E. Radmoser, O. Scherzer, and J. Weickert. Scale–space properties of regularization methods. In M. Nielsen, P. Johansen, O. F. Olsen, and J. Weickert, editors, *Scale-Space Theories in Computer Vision. Second International Conference, Scale-Space '99, Corfu, Greece, September 1999*, Lecture Notes in Computer Science; 1682, pages 211–220. Springer, 1999.
31. G. Sapiro. Vector (self) snakes: A geometric framework for color, texture, and multiscale image segmentation. In *Proc. IEEE International Conference on Image Processing, Lausanne*, September 1996.
32. A. Sarti, K. Mikula, and F. Sgallari. Nonlinear multiscale analysis of 3D echocardiography sequences. *IEEE Transactions on Medical Imaging*, 18(6):453–466, 1999.
33. J. A. Sethian. *Level Set Methods and Fast Marching Methods*. Cambridge University Press, 1999.
34. J. E. Taylor, J. W. Cahn, and C. A. Handwerker. Geometric models of crystal growth. *Acta metall. mater.*, 40:1443–1474, 1992.
35. J. P. Thirion. Image matching as a diffusion process: An analogy with maxwell's demon. *Medical Imag. Analysis 2*, pages 243–260, 1998.
36. V. Thomée. *Galerkin - Finite Element Methods for Parabolic Problems*. Springer, 1984.
37. J. Weickert. Anisotropic diffusion filters for image processing based quality control. In A. Fasano and M. Primicerio, editors, *Proc. Seventh European Conf. on Mathematics in Industry*, pages 355–362. Teubner, 1994.
38. J. Weickert. *Anisotropic diffusion in image processing*. Teubner, 1998.